

The collisions of high-velocity clouds with the galactic halo

Petr Jelínek^{a,b}, Gerhard Hensler^a

^a*University of Vienna, Institute of Astronomy, Türkenschanzstraße 17,
1180 Vienna, Austria*

^b*University of South Bohemia, Faculty of Science, Branišovská 10,
370 05 České Budějovice, Czech Republic*

Abstract

Spiral galaxies are surrounded by a widely distributed hot coronal gas and seem to be fed by infalling clouds of neutral hydrogen gas with low metallicity and high velocities. We numerically study plasma waves produced by the collisions of these high-velocity clouds (HVCs) with the hot halo gas and with the gaseous disk. In particular, we tackle two problems numerically: 1) collisions of HVCs with the galactic halo gas and 2) the dispersion relations to obtain the phase and group velocities of plasma waves from the equations of plasma motion as well as further important physical characteristics such as magnetic tension force, gas pressure, etc. The obtained results allow us to understand the nature of MHD waves produced during the collisions in galactic media and lead to the suggestion that these waves can heat the ambient halo gas. These calculations are aiming at leading to a better understanding of dynamics and interaction of HVCs with the galactic halo and of the importance of MHD waves as a heating process of the halo gas.

Keywords: Numerical simulations, high-velocity clouds, plasma waves, dispersion relations

1. Introduction

Spiral galaxies are surrounded by hot coronal gas for whose existence three main origins are under debate: 1) Most plausibly, star-formation activity in the galactic disk (stellar wind and supernova type II explosions) pushes hot gas into the halo, by this, producing the hot-gas halo [1, 2]. 2) Galaxy growth within the Λ CDM cosmology will inherently lead to gas accretion and by this produce a hot halo with virial temperatures if the cooling time is too long as for temperatures above 10^6 K and thus for large galactic masses of $M > 10^{11} M_{\odot}$. 3) And at least, cosmological simulations suggest that 30 – 40% of all baryons reside in a cosmic web of shock-heated warm-to-hot intergalactic medium accumulating as an extended hot halo around massive galaxies [3].

Another gas phase existing in the halo of spiral galaxies are high-velocity clouds (HVCs). In the

Milky Way these gas complexes are detected in HI at high galactic latitudes [4] and are falling with high speeds towards the galactic disk. Since galactic halo gas is preferentially assumed to be produced through the above-mentioned process 1), some of this hot gas is suggested to condense, cool [5], and to fall back to the galactic plane, or HVCs can stem directly from galactic HI gas that is swept-up by superbubbles, lifted into the halo, and returns on ballistic trajectories. While the first is, however, contradicted by Binney and collaborators [6] because of heat conduction, the second process would require also positive HI cloud velocities which are, however, not observed.

This expected galactic fountain effect [7] can, however, not explain HVC velocities close or even above the galactic escape value. Moreover, HVCs contain clearly less than solar metal abundances and have probably larger distances [8, 9] than achievable from

superbubble expansion, so that their origin from the galactic disk is very unlikely. In addition, there also exists a population of intermediate velocity HI clouds (IVCs). With their higher metallicity and far lower velocity of only $50 - 100 \text{ km} \cdot \text{s}^{-1}$ these clouds as well as those even slower (and smaller), so-called low-velocity clouds (LVCs), are also likely to reflect at least partly back-falling bullets expected from a galactic fountain.

A not insignificant part of LVCs, however, can be assumed to have passed the galactic halo and is decelerated by the drag of the ram pressure exerted by the hot halo gas [10]. This also leads to gas stripping from the clouds which is discernible as head-tail structure of HVCs [11]. As observed in several HVCs before and expected theoretically [12], the HVC 125+41-207 shows a two-phase structure with a low and high velocity dispersion for column densities larger than $2 \times 10^{15} \text{ m}^{-2}$.

Since in external galaxies seen edge-on like e.g. NGC 891 and NGC 4361 the hot halo gas is permeated with vertical magnetic field lines, and because the galactic hot halo gas is assumed to be mostly replenished by superbubbles which open perpendicular to the gaseous disk and, by this, also open the galactic magnetic field perpendicularly as it is coupled to the ionized gas, HVCs must be assumed to interact with the halo magnetic field. Unfortunately, topology, strength, and signatures of the galactic magnetic field are not well known and not yet manifested by observations. Consequently, the magnetic coupling of HVCs with the halo magnetic field is still vague and not yet elaborated. This innocence is not only caused by uncertainty of the field topology but mainly due to the total absence of magnetic field measurements in HVCs.

Only Zimmer et al. [13] interpreted observations of X-ray gas connected with HVCs [14], and preferentially with the HVC complex C, as signatures of magnetic reconnection and explored the magnetic interaction of HVCs with the Reynolds layer [15]. Another and far more realistic interpretation of the multi-gas phase coincidence in HVCs is the sweep-up of hot halo gas by the large complexes on their passage through the halo. HVC models by Vieser & Hensler [16] in which the clouds survive the dis-

ruption by Kelvin-Helmholtz instability due to self-gravitation, heat conduction, and cooling, the gas accumulation from such surrounding hot gas has been demonstrated.

Subsequently, Santillan et al. [17] investigated the collision of HVCs with the magnetic galactic gas disk by means of 2D numerical models. In contrast to the model assumptions of both studies no HVCs, i.e. large cloud complexes with velocities of $-200 \text{ km} \cdot \text{s}^{-1}$ and below, are found close to the galactic disk. Another limitation is that the magnetic field (in 2D) is only directed parallelly to the galactic plane.

2. Motivation of the numerical study

One of the unsolved problems in solar plasma physics is the heating of the solar corona. There exist mainly two possible explanations of this interesting problem – magnetic energy releasing and heating by the reconnection of magnetic field and heating the solar corona by plasma waves. In recent years, both of possible mechanisms were solved by many authors theoretically and also numerically (see e.g. [18], [19] or [20]).

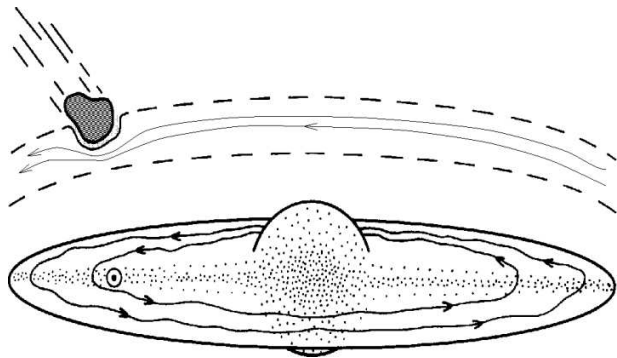


Figure 1: A HVC collides with the Reynolds layer, an ionized hydrogen layer of the galactic halo which includes magnetic fields. Picture taken and redrawn from [13].

Since superbubbles expanding into the halo are supposed to cool adiabatically and the halo gas should continue at lower temperature to cool by radiation and by cloud evaporation, a continuous hot gas

supply is necessary. Because of the complexity of the multi-phase gas structure of the halo there is still a lack of sufficiently detailed quantitative explorations and results about its thermodynamics and magnetohydrodynamics [21]. An additional heating source would therefore elegantly provide a solution to prevent the halo cooling. During the collisions of HVCs on trajectories oblique or perpendicular to the magnetized galactic halo or galactic disk, the magnetic field lines along the galactic disc are distorted [13], gas is compressed, and MHD waves are generated.

Such MHD waves (including reconnection of magnetic field) may, on one hand, lead to heating of the ambient gas and can, furthermore, influence the evolution and the dynamics of HVCs. This process is analogous to the coronal heating in the sun [22]. This similarity of MHD processes encourage us to begin analogous MHD studies of HVCs passing through the halo and approaching the galactic disk while interacting with the magnetic field.

3. Numerical model

3.1. Simulations of collisions of HVCs with galactic halo

In plasma physics, there exist several methods, how the plasma dynamics can be described and calculated, see e.g. [23], [24].

For the calculations of HVCs' dynamics we used the full set of MHD equations [25] with the addition of gravitational term:

$$\frac{\partial \varrho}{\partial t} = -\nabla \cdot (\varrho \mathbf{v}), \quad (1)$$

$$\varrho \frac{\partial \mathbf{v}}{\partial t} + \varrho (\mathbf{v} \cdot \nabla) \mathbf{v} = -\nabla p + \frac{1}{\mu_0} (\nabla \times \mathbf{B}) \times \mathbf{B} + \varrho \mathbf{g}, \quad (2)$$

$$\frac{\partial \mathbf{B}}{\partial t} = \nabla \times (\mathbf{v} \times \mathbf{B}), \quad (3)$$

$$\frac{\partial U}{\partial t} = -\nabla \cdot \mathbf{S}, \quad (4)$$

$$\nabla \cdot \mathbf{B} = 0. \quad (5)$$

Here ϱ is a mass density, \mathbf{v} (relative) flow velocity, p gas pressure, \mathbf{B} is the magnetic field and \mathbf{g} is the

gravitational acceleration calculated by means of Eq. (17).

The plasma energy density U is given by:

$$U = \frac{p}{\gamma - 1} + \frac{\varrho}{2} v^2 + \frac{B^2}{2\mu_0}, \quad (6)$$

with the adiabatic coefficient $\gamma = 5/3$, and the flux vector \mathbf{S} is expressed as:

$$\mathbf{S} = \left(U + p + \frac{B^2}{2\mu_0} \right) \cdot \mathbf{v} - (\mathbf{v} \cdot \mathbf{B}) \frac{\mathbf{B}}{\mu_0}. \quad (7)$$

The magnetohydrodynamic equations (1)-(4) were transformed into a flux conserving form, i.e.:

$$\frac{\partial \Psi}{\partial t} + \frac{\partial \mathbf{F}(\Psi)}{\partial x} + \frac{\partial \mathbf{G}(\Psi)}{\partial y} = 0, \quad (8)$$

and were solved numerically. The vector Ψ in our two-dimensional case is expressed as:

$$\Psi = \begin{pmatrix} \rho \\ \rho v_x \\ \rho v_y \\ B_x \\ B_y \\ U \end{pmatrix}. \quad (9)$$

The vector functions $\mathbf{F}(\Psi)$ and $\mathbf{G}(\Psi)$ are too complex to be presented here, for more information see e.g. [25].

For the numerical solution of this type of equations the two-step Lax-Wendroff algorithm is used. The numerical region is oriented in the x, y -plane, implemented at $0 \leq x \leq L$ and $0 \leq y \leq L$ and covered by a uniform grid with 200×200 cells. We choose the x coordinate to be oriented in the galactic plane, while y points vertically into the halo.

Open boundary conditions are applied and the time step satisfies Courant-Friedrichs-Levy condition in the form [25]:

$$\Delta t \leq \frac{\text{CFL} \cdot \Delta x}{\max(c_s + |\mathbf{v}|)}, \quad (10)$$

where the Courant number CFL is set to 0.8.

3.2. Calculations of phase and group speeds

For the calculations of phase and group velocities of plasma waves in the galactic gas, we numerically solve the wave equation for plasma motions, where the equilibrium parameters (density and pressure) depend on y (e.g. [26]):

$$\frac{d}{dy} \left[f(y) \frac{dv_y}{dy} \right] + \varrho(\omega^2 - k_x v_{\text{Alf}}^2) v_y = 0. \quad (11)$$

Here v_y is the velocity component normal to the magnetic field, ω is the frequency, k_x is the longitudinal wavenumber along the x -axis, and Alfvén speed $v_{\text{Alf}}^2 = B^2/\mu_0\varrho$.

The velocity v_x , parallel to the magnetic field is given by:

$$v_x = -\frac{ik_x c_s^2}{(\omega^2 - k_x^2 c_s^2)} \cdot \frac{dv_y}{dy}, \quad (12)$$

where $c_s = (\gamma p/\varrho)^{1/2}$ is the sound speed.

The function $f(y)$ from Eq. (11) is expressed as:

$$f(y) = \frac{\varrho c_f^2 (\omega^2 - k_x^2 c_T^2)}{(\omega^2 - k_x^2 c_s^2)}. \quad (13)$$

The tube speed c_T and fast speed c_f are implied as $c_T = c_s v_{\text{Alf}} / (c_s^2 + v_{\text{Alf}}^2)^{1/2}$ and $c_f = (c_s^2 + v_{\text{Alf}}^2)^{1/2}$, respectively.

Eq. (11) has a singular point which is called the cusp resonance or cusp singularity. This point plays an important role in a case of slow magnetoacoustic waves, whereas it is not seen in numerical simulations of the fast magnetoacoustic waves (e.g. [27]).

The second-order ordinary differential equation is rewritten in terms of two first-order equations of the new functions ξ_1 and ξ_2 :

$$\xi_1 = f(y) \frac{dv_y}{dy}, \quad \xi_2 = v_y, \quad (14)$$

such that:

$$\frac{d\xi_1}{dy} = \varrho(k_x v_{\text{Alf}}^2 - \omega^2) \xi_2, \quad \frac{d\xi_2}{dy} = \frac{\xi_1}{f(y)}. \quad (15)$$

The boundary conditions at the point $y = 0$ for the “kink” mode are given by $\xi_1 = 0, \xi_2 = c$ and

the “sausage” mode satisfies the boundary conditions $\xi_1 = c \cdot f(0), \xi_2 = 0$, whereas the constant c is arbitrary.

To obtain a solution of Eq. (11) a fixed value of k_x is used, integrating between $y = 0$ and $y = y_{\text{max}}$ the two first-order differential equations (14) and (15) by means of the fourth-order Runge-Kutta method. Exact value of the frequency ω is obtained by the bisection iteration method when the velocity v_y satisfies the boundary condition at the second point $v_y(y = y_{\text{max}}) = 0$ for both wave modes (“kink” and “sausage” mode).

The total gas pressure p_{tot} (gas and magnetic) is expressed as:

$$\frac{i\omega}{\varrho} p_{\text{tot}} = -\frac{c_f^2 (\omega^2 - k_x^2 c_T^2)}{(\omega^2 - k_x^2 c_s^2)} \frac{dv_y}{dy}, \quad (16)$$

and for the calculation of the magnetic tension force \mathbf{T}_1 we use the equation in the form, see [26]:

$$\frac{i\omega}{\varrho} \mathbf{T}_1 = (\omega^2 - k_x^2 c_s^2) \frac{v_{\text{Alf}}^2}{c_s^2} \hat{\mathbf{e}}_x - v_{\text{Alf}}^2 k_x^2 v_y \hat{\mathbf{e}}_y. \quad (17)$$

This force is a part of the Lorentz force $\mathbf{j} \times \mathbf{B}$ and appears whenever the magnetic field lines are curved. Magnetic tension force is determined by how much the magnetic pressure changes with distance (for detailed information see [26]).

4. Initial conditions

4.1. Collisions of HVCs with galactic halo

Numerical solutions of MHD equations are performed in 2D space. The absolute size of the simulation box amounts 3 kpc \times 3 kpc. The initial position of modeled HVC is located 1250 pc above the galactic plane with an initial velocity of $v_0 = -200 \text{ km} \cdot \text{s}^{-1}$ [17].

The mass density distribution of the galactic gas is given by the equation:

$$\begin{aligned} \varrho(y) &= \varrho_0 [0.6e^{-y^2/(280\text{pc})^2} + 0.37e^{-y^2/(540\text{pc})^2} + \\ &+ 0.1e^{-|y|/400\text{pc}} + 0.03e^{-|y|/900\text{pc}}], \end{aligned} \quad (18)$$

and for the expression of the gravitational acceleration we use the equation [17]:

$$g(y) = 8 \cdot 10^{-7} [1 - 0.52e^{-|y|/325\text{pc}} - 0.48e^{-|y|/900\text{pc}}] \text{ m} \cdot \text{s}^{-2}. \quad (19)$$

The galactic midplane gas density in Eq. (18) is $\rho_0 = 2.24 \times 10^{-21} \text{ kg} \cdot \text{m}^{-3}$ and the initial magnetic field $B_0 = 5.0 \mu\text{G}$. The total pressure is given by the relation $p(y) = \int \rho g dy$, with the boundary condition that $p_{\text{out}} = p(y = 5.0 \text{ kpc}) = 0 \text{ Pa}$. The galactic midplane value of the total pressure $p_0 = 2.7 \times 10^{-13} \text{ Pa}$ [17].

4.2. Phase and group speeds

For both studied cases (uniform magnetic field parallel to the galactic plane and galactic current sheet configuration), we assume, in the state of equilibrium, initial plasma velocity $\mathbf{v} = 0$.

Equilibrium demands that the pressure (plasma plus magnetic) is uniform, i.e.:

$$p + \frac{B^2}{2\mu_0} = \text{const.} \quad (20)$$

4.2.1. Uniform magnetic field

In this case, the magnetic field is assumed $\mathbf{B} = B_0 = \text{const.}$ in the whole simulation region. The total pressure p according to the Eq. (20) is also assumed to be a constant, $p = p_0$.

4.2.2. Current sheet

In the case of current sheet configuration the magnetic field is given by the equation [18]:

$$\mathbf{B} = B_0 \tanh \left[\frac{(y - L/2)}{a} \right] \hat{\mathbf{e}}_{\mathbf{x}}, \quad (21)$$

and the equilibrium in Eq. (18) yields a plasma pressure given by:

$$p(y) = p_0 \text{sech}^2 \left[\frac{(y - L/2)}{a} \right], \quad (22)$$

given that $p \rightarrow 0$ (cold plasma) as $(|y|/a) \rightarrow \infty$ [26], and where $a = 0.5 \text{ kpc}$ is the semi-width of the current sheet.

Numerical solutions of Eq. (11) are performed only for the so-called ‘‘kink’’ mode [26], which well corresponds to the situation of the HVC collision with galactic disk.

5. Results and discussions

In this section we present some selected numerical results obtained by means of our simulations.

5.1. Collisions of HVCs with galactic halo

In Figs. 2 and 3 we present the ‘‘time evolution’’ of a HVC collision with galactic media. Fig. 2 shows the perpendicular collision, whereas in Fig. 3 an oblique passage of the HVC with $\alpha = 45^\circ$ through the galactic halo is depicted.

The situations (a) show the gas density distribution at the ‘‘beginning’’, i.e. $T_a = 0.6 \text{ Myr}$ after the onset of the calculation, while the locations (b) present the density distributions for the time $T_b = 7.9 \text{ Myr}$ in the case of perpendicular collision (Fig. 2) and $T_b = 12.8 \text{ Myr}$ for oblique cloud infall (Fig. 3).

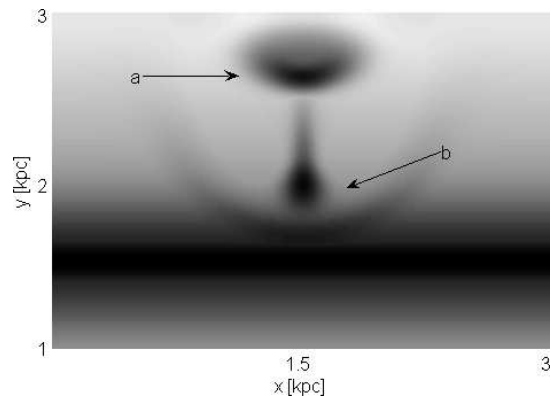


Figure 2: The ‘‘time evolution’’ of the collision of HVCs with galactic halo in the case of perpendicular cloud infall. a: cloud at 0.6 Myr after the start of the models, b: position and structure at time T_b (see text).

In both cases at time T_b a dense regime in front of the HVC is clearly visible, where the galactic gas is

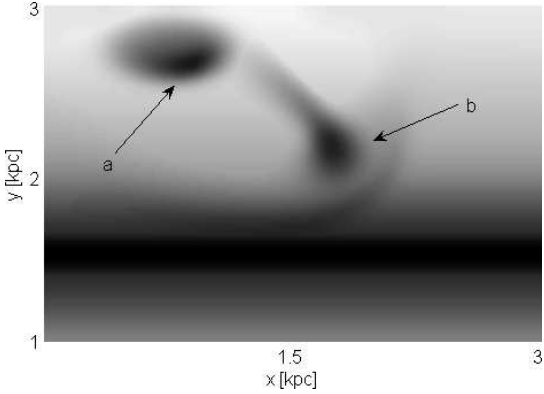


Figure 3: The “time evolution” of the collision of HVCs with galactic halo in the case of oblique cloud infall under $\alpha = 45^\circ$. a: cloud at 0.6 Myr after the start of the models, b: position and structure at time T_b (see text).

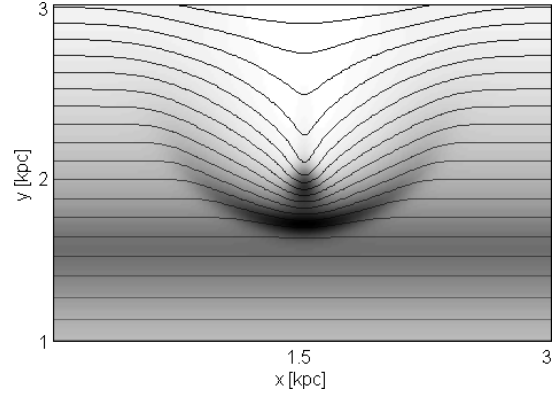


Figure 4: The total pressure in the numerical region and magnetic field lines distorted by the HVC for the perpendicular infall of the cloud to the galactic disk at time T_b (see text).

compressed as the HVC moves towards denser galactic disk and is decelerated.

Because this infall motion towards denser gas causes a bow shock to form, consequently, also plasma waves are created.

In Figs. 4 and 5 are shown the total pressure of the galactic gas and magnetic field lines for both studied cases, i.e. perpendicular and oblique infall under angle $\alpha = 45^\circ$. The pressure on the head of the cloud is higher because the cloud moves through gas with increasing density near galactic disk, and the magnetic field lines are distorted because the magnetic field is “frozen” to the HVC.

5.2. Phase and group speeds

In Figs. 6 and 7 we present the phase and group speeds of wave signal, plasma velocity, total gas pressure and magnetic tension force for magnetic field oriented parallelly to the galactic plane and for a current sheet configuration, respectively.

Notice, that in the graph of the phase and group speeds the scale on the left-hand side corresponds to the phase speed (solid line), whereas the scale on the right-hand side corresponds to the group speed (dash-dotted line) of the plasma waves. If we compare the phase and group speeds for both studied cases, we

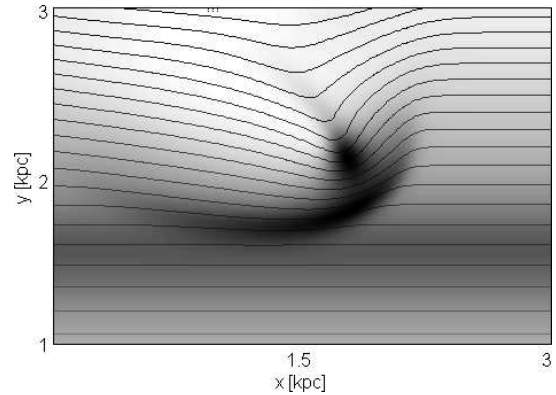


Figure 5: The total pressure in the numerical region and magnetic field lines distorted by the HVC for the oblique infall ($\alpha = 45^\circ$) of the cloud to the galactic disk at time T_b (see text).

can see that the profiles of phase speeds are similar, whereas the group speeds have different shapes. In the case of the current sheet the group speed becomes constant for high wavenumbers.

From the figures of total pressure p_{tot} we can discern that for $k_x a = 5$ (red line) the lines are also the same, whereas for $k_x a = 10$ (blue line) the total pressure is zero outside of current sheet, because of

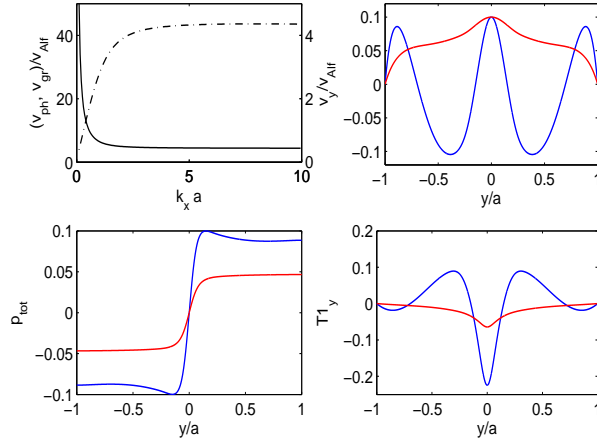


Figure 6: Phase (solid) and group (dash-dotted) velocity of wave signal (upper left); plasma velocity component v_y (upper right), total gas pressure (bottom left) and magnetic tension force (bottom right) for magnetic field oriented parallelly to the galactic plane, wavenumbers $k_x a = 5$ (red) and $k_x a = 10$ (blue).

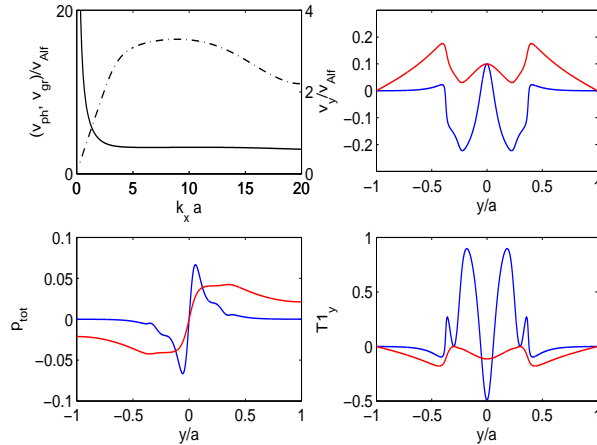


Figure 7: Phase (solid) and group (dash-dotted) velocity of wave signal (upper left); plasma velocity component v_y (upper right), total gas pressure (bottom left) and magnetic tension force (bottom right) for the current sheet configuration, wavenumbers $k_x a = 5$ (red) and $k_x a = 10$ (blue).

constant (zero) plasma velocity v_y , see Eq. (16).

For the plasma velocity component v_y in Fig. 7 it is clearly visible, where the edge of the current sheet

is located. Outside of the current sheet the plasma velocity is zero for $k_x a = 10$ and falls to zero in case of $k_x a = 5$. This means that practically only the part of the galactic gas, where the magnetic field is not constant, is moving. In the case of a parallel magnetic field, galactic gas moves over the whole simulation region. It is probably caused by the fact, that inside the current sheet is present the Lorentz force $\mathbf{j} \times \mathbf{B}$ which does not allow the plasma waves generated in the center of the current sheet leave freely this space.

As one can see, the y -component of the magnetic tension force \mathbf{T}_1 is in “anti-phase” to the plasma y -velocity component in all cases.

6. Conclusions

Our main aim is to investigate the effects of the collisions of HVCs with both the galactic media, hot halo gas and magnetic field, on their descendance towards the galactic disk. For this purpose here we present a first insight with respect to two aspects by 2D numerical models: at first, we solve numerically the set of MHD equations and simulate the collisions of HVCs with the galactic media for two cases (oblique and perpendicular collision). In the second part of this paper, the equation of plasma motion is treated numerically in order to obtain the dispersion relations of waves in galactic media.

In the literature [13] it is envisaged that the reconnection of magnetic field lines in the galactic halo can lead to its gas heating. Unfortunately, but as a physically reasonable by-product, heating of the halo gas by plasma waves is not yet taken into account. There exists practically no paper dealing with this interesting problem.

Our first results demonstrate that plasma waves provide an important heating process of the galactic halo gas in analogy to the solar corona. From the above-mentioned reasons our results are new and their further exploration of crucial importance for our understanding of the heating processes in the interstellar medium in general. Nevertheless, 2D simulations can only deal as a first insight but 3D simulations are urgent for the MHD treatment to deliver more accurate and reliable results. Therefore, as the next step we will advance our models to 3D

and to higher spatial resolution. For this purpose we intend to use as a powerful, well tested and widely applied tool for astrophysical simulations of many applications the FLASH code [28], parallelized and with adaptive mesh refinement. Recently, [29] performed first 3D models using FLASH, but with the main emphasis on the structural evolution of fountain clouds starting at a height of 5 kpc above the galactic disk. From the extension of our numerical models we expect important results and information about the MHD waves in galactic media. As further steps, also small-scale plasma processes like heat conduction must be included, that leads to the stabilization of clouds [16] by suppression of KH instability.

Acknowledgements

This research has been funded by the University of Vienna, partly within the priority programme “Computer-aided Sciences” under grant No. FS538001.

P.J. acknowledges partial financial support of the grant P209/10/1680 of the Grant Agency of the Czech Republic.

The authors thank the anonymous referee for valuable comments which improve the quality of the paper.

References

- [1] Strickland, D.K., et al., ApJ 606 (2004) 829.
- [2] Tüllmann, R., et al., A&A 448 (2006) 43.
- [3] Rasmussen, J., et al., ApJ 697 (2009) 79.
- [4] Wakker, B.P. & van Woerden, H., ARA&A 35 (1997) 217.
- [5] Collins, J.A., Shull, J.M., & Giroux, M.L., ApJ 623 (2005) 196.
- [6] Binney, J., Nipoti, C., & Fraternali, F., MNRAS 397 (2009) 1804.
- [7] Shapiro, P.R. & Field G. B., ApJ 205 (1976) 762.
- [8] Wakker, B.P., ApJS 136 (2001) 463.
- [9] Wakker, B.P., et al., ApJ 672 (2008) 298.
- [10] Benjamin, R.A. & Danly, L., ApJ 481 (1997) 764.
- [11] Brüns, C. et al., A&A 357 (2000) 120.
- [12] Wolfire, M.G. et al., ApJ 453 (1995) 673.
- [13] Zimmer, F., Lesch, H., Birk, G. T., A&A 320 (1997) 746.
- [14] Kerp, J. et al., A&A 312 (1996) 67.
- [15] Reynolds, R.J., Roesler, F.L., & Scherb, F., ApJ 192 (1974) L53.
- [16] Vieser, W. & Hensler, G., A&A 475 (2007) 251.
- [17] Santillán, A., Franco, J., Martos, M., Kim, J., ApJ 515 (1999) 657.
- [18] Kliem, B., Karlický, M., Benz, A. O., A&A 360 (2000) 715.
- [19] Jelínek, P., & Karlický, M., Eur. Phys. J. D 54 (2009) 305.
- [20] Jelínek, P., & Karlický, M., IEEE Trans. Plasma Sci. 38(9) (2010) 2243.
- [21] Henley, D.B., et al., ApJ 723 (2010) 935
- [22] Hirth, W., & Krüger, A., A&A 354 (2000) 365.
- [23] Jelínek, P., Šimek, J., Hrach, R., Czech. J. Phys. 56 (2006) B809B814.
- [24] Šimek, J., Hrach, R., Jelínek, P., Comp. Phys. Commun. 177 (2007) (1-2).
- [25] Chung, T. J., Computational Fluid Dynamics, Cambridge University Press, New York USA, 2002.
- [26] Smith, J. M., Roberts, B., Oliver, R., A&A 327 (1997) 377.
- [27] Zhukov, V. I., Astrophys. Space Sci. 154 (1989) 247.
- [28] Fryxell, B., et al., ApJS 131 (2000) 273.
- [29] Kwak, K., Shelton, R.L., & Raley, E.A., ApJ 699 (2009) 1775.